Insight into the Structure-Dependent Effects of Metal Residues in Conjugated Polymers

Fanghua Zeng[a], Yudi Feng[a], Jiali Wang[a], Yanfeng Lin[a], Rui Xiong*[a], Dapeng Wu[b] and Can Yang*[a]

[a] State Key Laboratory of Photocatalysis on Energy and Environment, Fuzhou University, Fuzhou, Fujian, 350108, P. R. China

[b] Collaborat Innovat Ctr Henan Prov Green Mfg Fine C, Key Lab Yellow River & Huai River Water Environm, Henan Normal University, Xinxiang, Henan, 453007, P. R. China

* **Corresponding authors:** Email: rxiong421@163.com (R. Xiong); canyang@fzu.edu.cn (C. Yang)

1. Experimental section

Text S1 Chemicals and materials

All reagents used in the experiment are analytically pure and no further purification is required. 2,6-Dibromopyridine ($C_5H_3Br_2N$, 98.0%), 2,4-Dibromopyridine ($C_5H_3Br_2N$, 98.0%), 3,5-Dibromopyridine ($C_5H_3Br_2N$, 98.0%), Bis (triphenylphosphine) palladium(II) dichloride ($C_{36}H_{30}Cl_2P_2Pd$, 98.0%), CuI (99.5%), Toluene (C_7H_8, 99.5%), Diisopropylamine ($C_6H_{15}N$, 99.0%), Ethynyltrimethylsilane ($C_5H_{10}Si$, 98.0%), Ethyl acetate, ($C_4H_8O_2$, 99.8%), $MgSO_4$ (98.0%), Methanol (CH_4O, 99.9%), Tetrahydrofuran (C_4H_8O, 99.0%), NaOH (98.0%), n-Hexane (C_6H_{14}, 99.0%), Dichloromethane (CH_2Cl_2, 99.8%), Silica gel, 1,4-Dibromobenzene ($C_6H_4Br_2$, 98.0%), Tetrakis (triphenylphosphine) palladium ($C_{72}H_{60}P_4Pd$, 99.0%), N,N-Dimethylformamide (C_3H_7NO, 99.9%), Chloroform ($CHCl_3$, 99.5%), Acetone (C_3H_6O, 99.0%), Ethylenediaminetetraacetic acid ($C_{10}H_{16}N_2O_8$, 99.0%) were purchased from Sinopharm Chemical Reagent Co., Ltd (Shanghai, China). Ultrapure water (18 MΩ·cm) was used in all experiments.

Text S2 Synthesis of Py-X

2,6-Dibromo pyridine, 2,4-Dibromo pyridine and 3,5-Dibromo pyridine (5.01 g, 21.2 mmol) were mixed with $PdCl_2(PPh_3)_2$ (0.16 g, 0.2 mmol) and CuI (0.04 g, 0.2 mmol), respectively. The mixture was dissolved in the minimum amount of toluene (60 mL), DIPA (20 mL) and Ethynyltrimethylsilane (10 mL). After degassing with argon gas for 15 min, the reaction mixture was heated to 70 °C and stirred overnight. The solvent was removed, while the crude product was redissolved in ethyl acetate and washed with water (50 mL x 3). The organic phase was dried over $MgSO_4$ and the solvent was removed to obtain three brown solids designated as Py-1-TMS, Py-2-TMS and Py-3-TMS, respectively.

Under aerobic conditions, the previously formed Py-1-TMS, Py-2-TMS and Py-3-TMS were dissolved in a mixed solvent of methanol/THF (75 mL:75 mL), respectively. 1 M

NaOH (aq) (20 mL) was added, and the reaction mixture was stirred at room temperature for 2 h. Then, the solvent was removed and the obtained precipitate was redissolved in a mixed solvent of hexane/ethyl acetate (1:1). The organic phase was washed with brine (300 mL) and dried over $MgSO_4$. The brown crude product was redissolved in the minimum amount of hexane: DCM (1:1) and purified by column chromatography (silica; n-hexane: DCM [1:1]). After removing the solvent, three white products were obtained and designed as Py-1, Py-2 and Py-3, respectively.

Text S3 Synthesis of BPy-X

Py-X (127.0 mg, 1.0 mmol), 1,4-Dibromobenzene (236.0 mg, 1.0 mmol), $Pd(PPh_3)_4$ (12 mg) and CuI (8 mg) were placed in NEt_3 (8 mL) and DMF (8 mL) in 50 mL round-bottom flask, which was degassed with argon gas for 15 min. Then the mixture was heated to 90 °C and stirred under argon for 72 h. The resulting polymer was filtered and washed with chloroform, acetone, water and methanol for several times. Then the polymer was further purified by Soxhlet extraction with methanol for 72 h. The resulting products were dried at 80 °C for 24 h and named as BPy-1 (291.4 mg, brownish-black solid powder), BPy-2 (252.3 mg, brown solid powder) and BPy-3 (283.5 mg, dark yellow solid powder), respectively.

Text S4 Synthesis of BPy-1-PT

50 mg of BPy-1 was dispersed in an EDTA solution (0.01 M, 30 mL), sonicated for 10 min, and stirred at room temperature for 10 h. Subsequently, the product was separated from the solution by centrifugation and washed with deionized water for three times. Finally, the final brown solid powder was obtained after drying at 80 °C in a vacuum overnight and named as BPy-1-PT.

Text S5 H_2S adsorption test

The H_2S adsorption test was conducted in a glass tube with an inner diameter of 6 mm at 298 K. In a typical adsorption process, 5 mg of sample was added and controlled with the flow velocity of 20 ppm H_2S balanced with N_2 as 10 mL•min^{-1}. The concentration of H_2S was detected by a gas chromatography equipped with a pulsed flame photometric detector. The absorption pool containing the solution of NaOH was equipped to absorb the tail gas after the GC.

Text S6 Photocatalytic experiments

The photocatalytic oxidation of H_2S was carried out in a fixed-bed quartz photoreactor under atmospheric pressure. Firstly, 5 mg sample was ground with a certain amount of treated silicon dioxide in a mortar to keep the dosage of the catalysts fixed. Then, the mixture was filled in our self-designed quartz photoreactor, the irradiated area of which was about 1.5 cm^2 (1.5 cm × 1 cm). The gaseous reactant (20 ppm H_2S, 10% O_2, total flow rate = 10 mL min^{-1}, N_2 as balance) was constantly induced into the reaction system during the reaction. After the adsorption of H_2S saturated (the measured concentration of H_2S in the tail gas was about 20 ppm), the catalyst was irradiated by a 420 nm LED lamp (the distance between the lamp bead and the reaction window was about 1.2 cm), and the gaseous products were tested on-line by a gas chromatograph with a flame photometric detector. The photocatalytic reaction was displayed as followed.

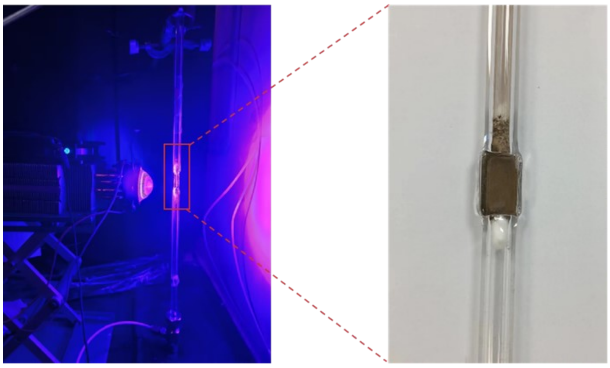

Text S7 Photoelectrochemical measurements

2 mg of the sample was added into 1 mL DMF, and the mixture was sonicated for 30 min. Then, 5 μL DMF dispersion was dropped on the cleaned FTO and the cover area was constrained within 1cm^2. The working electrodes was prepared after repeating the procedure once. The photoelectrochemical experiments were performed on Bio-Logic

VSP-300 electrochemical workstation using 0.2 M Na_2SO_4 as electrolyte, Ag/AgCl electrode as a reference electrode (in saturated KCl aqueous solution) and 14 cm^2 Pt electrode as a counter electrode.

Text S8 Radical trapping experiments

2 mg of catalyst were dispersed in 10 mL absolute methanol and sonicated for 30 min. For the detection of $\bullet O_2^-$, DMPO was used and prepared in 100 mM aqueous solution. The resulting suspension was then placed into a capillary and subjected to ESR instrument under both dark condition and light condition.

Text S9 Computational details

All density functional theory (DFT) calculations were performed by using the Gaussian 16 software.[1] Geometric configurations were optimized at the B3LYP level with a 6-311++G (d,p) basis set under gas-phase conditions.[2] The GD3BJ correction was used for all calculations. The formation energy of Cu doping on BPy-X can be defined as:

$$E_{form}=E_{Cu\text{-}BPy\text{-}X}-E_{BPy\text{-}X}-E_{Cu}$$

where $E_{Cu\text{-}BPy\text{-}X}$ is the total energy of Cu-BPy-X, $E_{BPy\text{-}X}$ is the total energy of BPy-X and E_{Cu} is the chemical potential of Cu crystal.

Text S10 Characterization methods

The Fourier transform infrared (FT-IR) spectra were obtained on a Thermo Nicolet iS50 spectrometer with DTGS ATR detector. Solid-state ^{13}C CP/MAS NMR tests were performed on a Bruker SB Avance III 500 MHz spectrometer. X-ray absorption fine structure (XAFS) spectra at the Cu K-edge were at BL14W beamline in Shanghai Synchrotron Radiation Facility (SSRF). The X-ray powder diffraction (XRD) measurements were performed on a Rigaku MiniFlex 600 diffractometer with CuKα1 radiation (λ = 1.5406 Å, 40 kV). The actual amount of Cu of CPs was determined on the inductive coupled plasma emission spectrometer (ICP, PerkinElmer Avio 200 Avio

200). The microstructures of the samples were observed by scanning electron microscope (SEM, FEI Nova NanoSEM 230). Brunauer-Emmett-Teller (BET) surface area and pore size measurements were recorded on a Micromeritics ASAP 2020M instrument at 77 K. The Raman spectra were recorded by a LabRAM HR Evolution Raman spectrometer system under 633 nm. Electron paramagnetic resonance (EPR) spectra were obtained from a Bruker model A 300 spectrometer. X-ray photoelectron spectroscopy (XPS, Thermo ESCALB 250Xi) with an Al Kα source was applied to explore the surface elements and the chemical state. The in-situ spectrum was recorded on Thermo Scientific Nicolet iS50 spectrometer at 64 scans per spectrum at a 4 cm^{-1} resolution. Temperature-programmed desorption of H_2S (H_2S-TPD) and O_2 (O_2-TPD) were investigated on Micromeritics AutoChem II 2920 Chemisorption Analyzer.

Text S11 The detailed photocatalytic pathways of BPy-1 toward H_2S

$$\mathrm{BPy-1} \xrightarrow{hv} h^+ + e^- \quad (1)$$

$$O_2 + e^- \longrightarrow \bullet O_2^- \quad (2)$$

$$H_2S \longrightarrow HS^- + H^+ \quad (3)$$

$$HS^- + \bullet O_2^- \longrightarrow S^* + OH^- \quad (4)$$

$$OH^- + H^+ \longrightarrow H_2O \quad (5)$$

$$\bullet O_2^- + S^* + H_2O \longrightarrow S / SO_2 / SO_4^{2-} + H^+ \quad (6)$$

2. Supplementary data

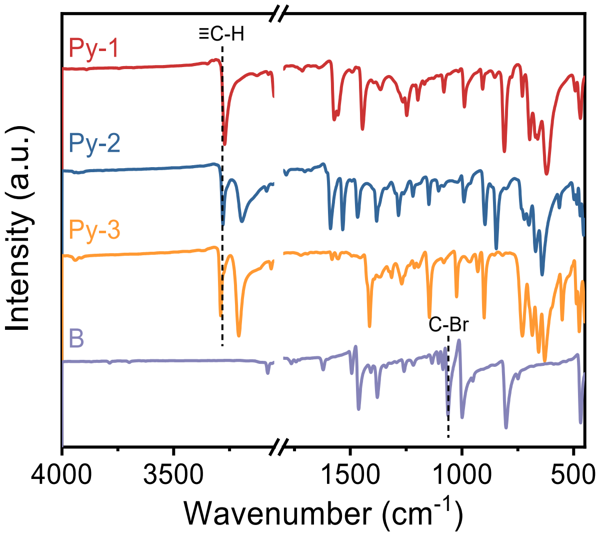

Fig. S1. The FTIR patterns of amino precursors (B and Py-X).

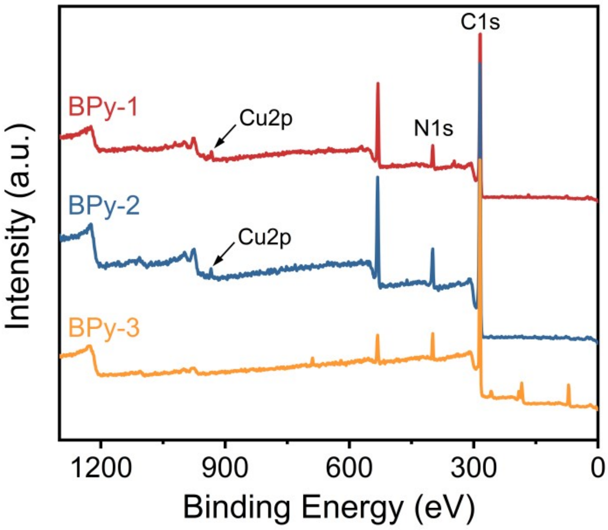

Fig. S2. The full XPS Spectrum of BPy-X.

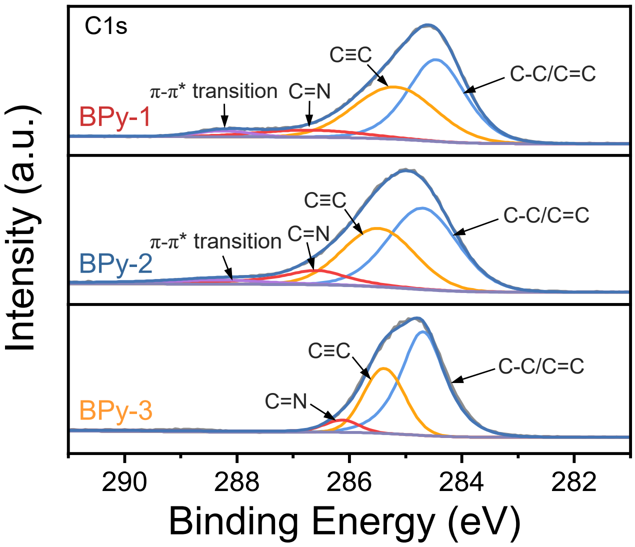

Fig. S3. C 1s XPS spectrum of BPy-X.

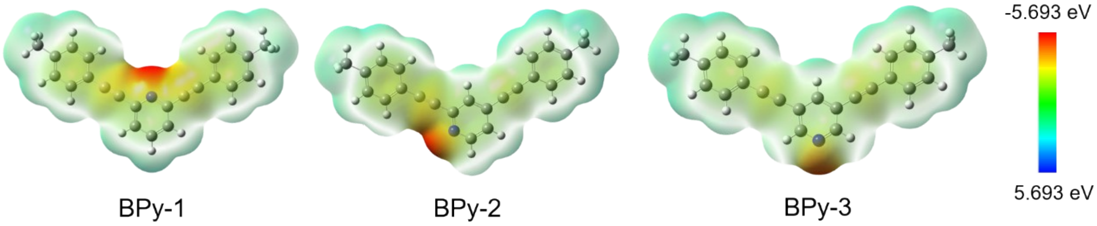

Fig. S4. ESP area distributions of BPy-1, BPy-2 and BPy-3 (The gray, white and blue cyan balls represent C, H and N atoms, respectively).

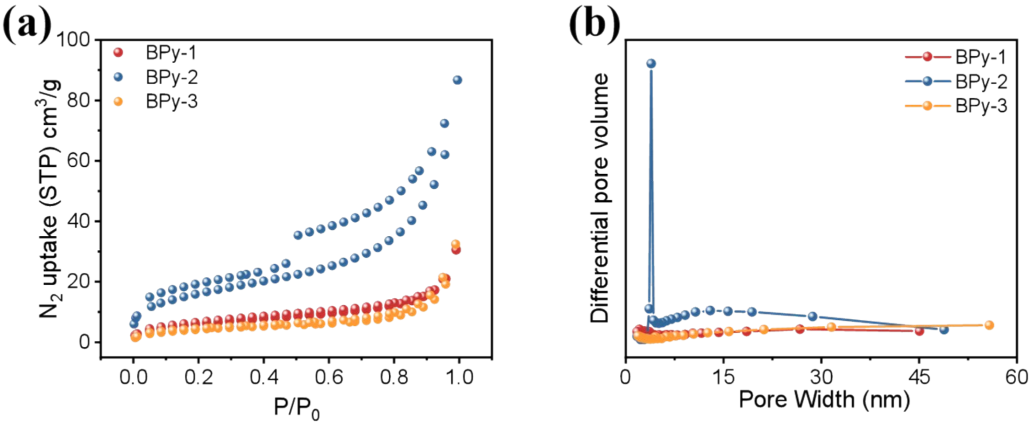

Fig. S5. (a) N_2 adsorption-desorption spectra; (b) pore size distribution spectra of BPy-1, BPy-2 and BPy-3.

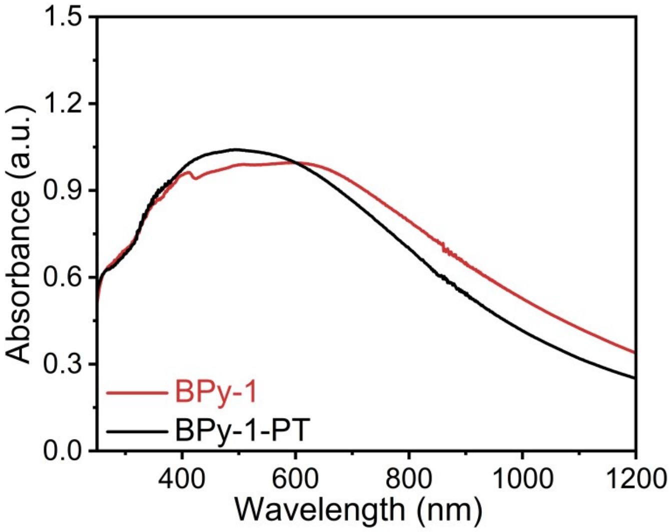

Fig. S6. UV-vis diffuse reflectance spectra of BPy-1and BPy-1-PT.

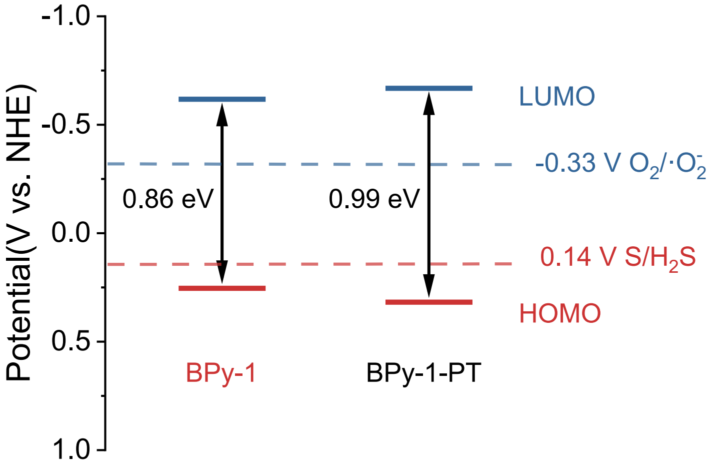

Fig. S7. Optical gap structure of BPy-1 and BPy-1-PT.

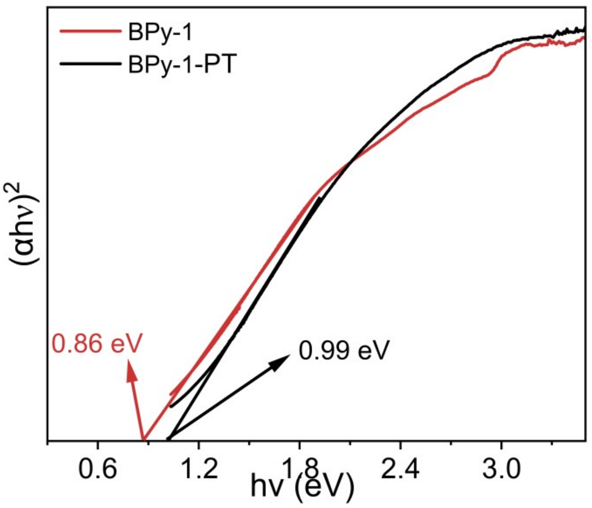

Fig. S8. Tauc plots curve of BPy-1 and BPy-1-PT.

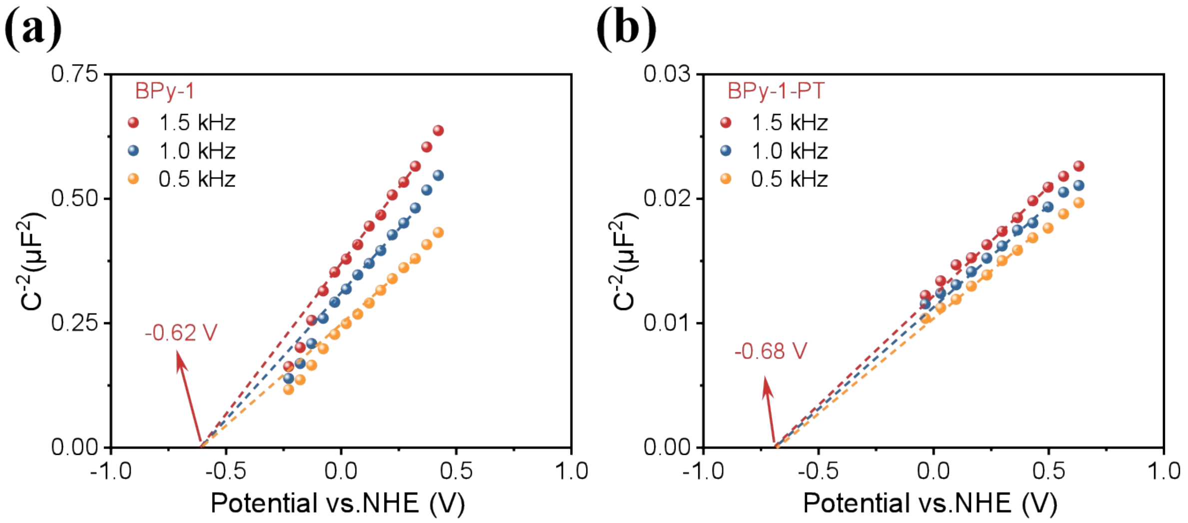

Fig. S9. Mott-Schottky plots of the polymers (a) BPy-1 and (b) BPy-1-PT.

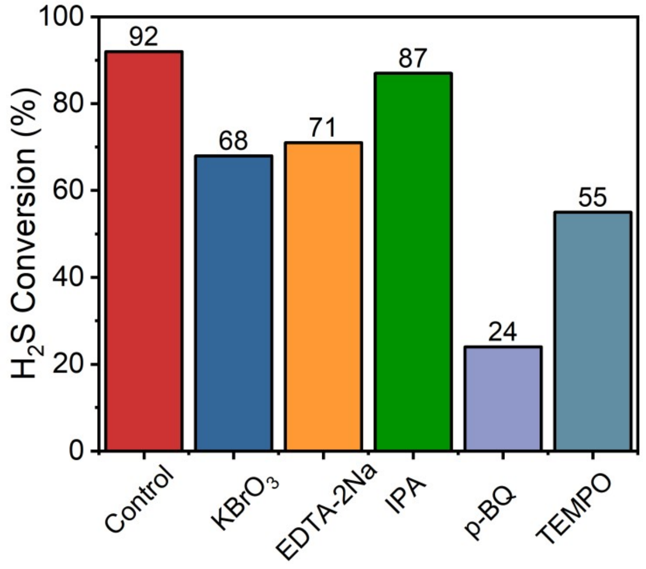

Fig. S10. Effect of radical scavengers on BPy-1 in photocatalytic oxidation of H_2S.

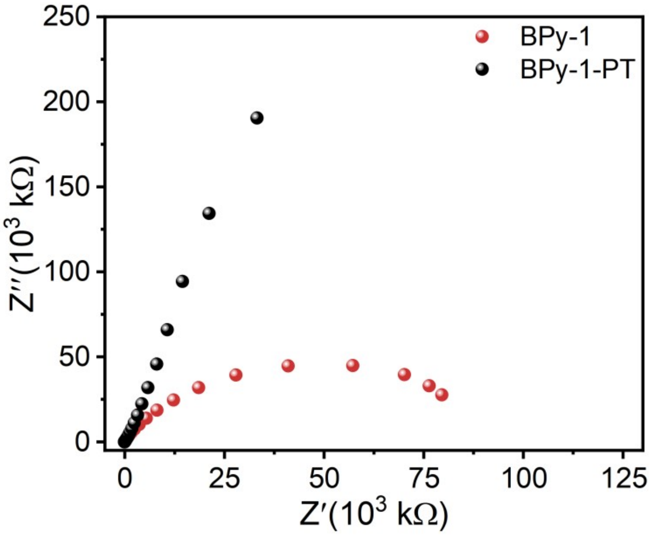

Fig. S11. The electrochemical impedance spectroscopy of BPy-1 and BPy-1-PT.

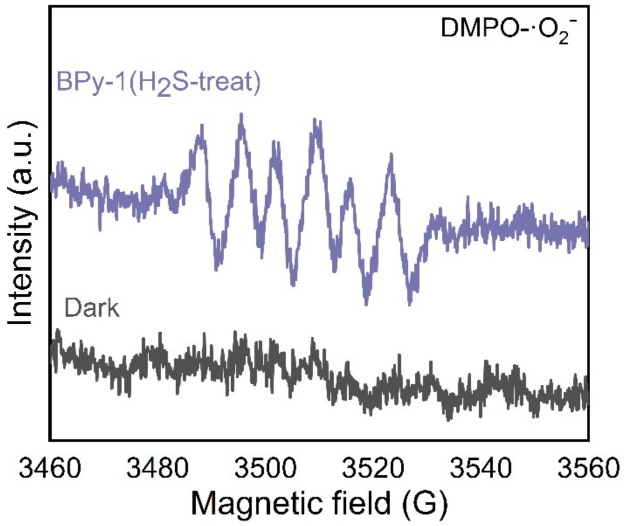

Fig. S12. DMPO-•O_2^- spectra of BPy-1(H_2S-treat).

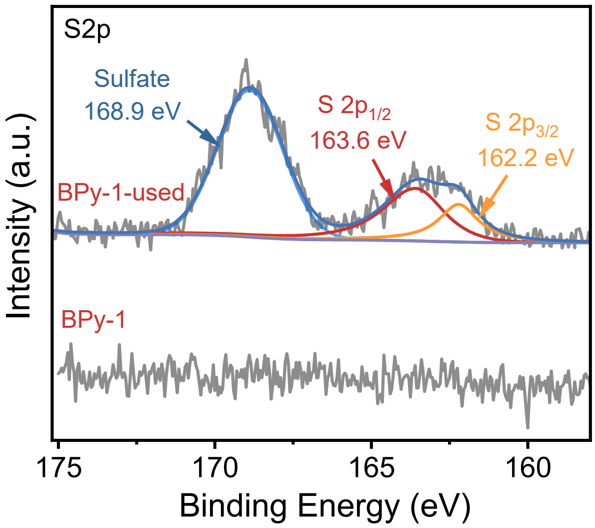

Fig. S13. S 2p XPS spectrum of BPy-1 before and after the test.

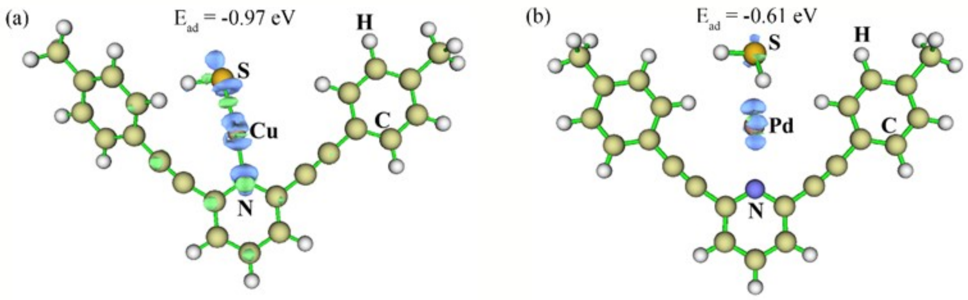

Fig. S14. The charge density difference of (a) Cu-BPy-1 and (b) Pd-BPy-1. The green and blue contours represent the electron accumulation and depletion, respectively. The isovalue is set to 0.005 e/Å^3.

DFT calculation is used to further explore the role of residual Cu and Pd in BPy-1 for H_2S adsorption. As shown in Fig. S14, the calculated adsorption energy of H_2S on Cu-BPy-1 is -0.91 eV, which is higher than Pd-BPy-1 (-0.61 eV). From the charge density difference results, it can be seen that the charge transfer between Cu and the adsorbed H_2S molecule in Cu-BPy-1 is more pronounced compared to that between Pd and H_2S in Pd-BPy-1. This indicates a stronger electronic interaction in the Cu-BPy-1 system, which facilitates the activation of the H_2S molecule. These theoretical results further support that residual Cu plays a critical role in enhancing the photocatalytic performance toward H_2S oxidation, while trace Pd residue is not the dominant factor influencing the photocatalytic H_2S oxidation.

Table S1. XPS analysis of BPy-X

Samples	Cu-N_x/C-N=C (at.%)	Summary N (at.%)	Cu (at.%)	Pd (at.%)
BPy-1	0.98	7.76	0.79	n.d.
BPy-2	0.67	8.23	0.46	n.d.
BPy-3	0.00	6.47	n.d.	n.d.

Table S2. Fitting results of Cu K-Edge EXAFS Data

Samples	Path	CN[a]	R(Å)[b]	σ^2(Å^2)[c]	ΔE_0(eV)[d]	R factor[e]
Cu foil	Cu-Cu	12 (fixed)	2.54±0.02	0.008	4.3±0.6	0.004
BPy-1	Cu-N	2.8	1.94±0.03	0.006	-3.0±3.7	0.018

R(Å)[b]: bond distance; CN[a]: coordination number; σ^2(Å^2)[c]: Debye-Waller factor; ΔE_0(eV)[d]: inner potential correction; R factor[e]: goodness of fit.

Table S3. The formation energy of Cu-BPy-X

Samples	Formation energy (eV)
Cu-BPy-1	-0.676
Cu-BPy-2	-0.647
Cu-BPy-3	-0.371

Table S4. BET and BJH results of BPy-X

Samples	SBET (m^2/g)	Pore volume (cm^3/g)	Average pore size (nm)
BPy-1	23	0.029	8.33
BPy-2	58	0.091	8.21
BPy-3	16	0.026	13.75

Table S5. ICP-OES analysis of the polymers and corresponding photocatalytic H_2S oxidation performance

Samples	Cu (wt.%)	Pd (wt.%)	H_2S Conversion (%)
BPy-1	1.42	0.22	92
BPy-2	1.21	0.35	78
BPy-3	0.09	0.15	49
BPy-1-PT	0.18	0.22	18

Table S6. ICP-OES analysis of BPy-1 for different post-treatment time and corresponding photocatalytic H_2S oxidation performance

Samples	Cu (wt.%)	Pd (wt.%)	H_2S Conversion (%)
BPy-1	1.42	0.22	92
BPy-1-PT_1	0.73	0.22	49
BPy-1-PT_2	0.18	0.22	18
BPy-1-PT_3	0.16	0.20	19

As shown in Table S5, we found that the concentrations of Pd are 0.22 wt%, 0.35 wt%, and 0.15 wt% for BPy-1, BPy-2 and BPy-3, respectively. However, despite BPy-2 exhibiting the highest Pd content, its photocatalytic H_2S conversion efficiency (78%) is lower than that of BPy-1 (92%). This trend suggests that the residual Pd does not positively correlate with photocatalytic activity and is unlikely to be the dominant contributor to PSO performance. Furthermore, we found that residual Cu species originating from CuI could be effectively removed via post-treatment with EDTA solution as the increase of processing time, as shown in Table S6. Interestingly, we observed a significant decrease in the H_2S conversion rate as the Cu content decreased, while the Pd content remained nearly unchanged. This phenomenon indirectly indicates that the residual Cu in our system plays a primary role in enhancing the photocatalytic activity.

3. Other results of structures

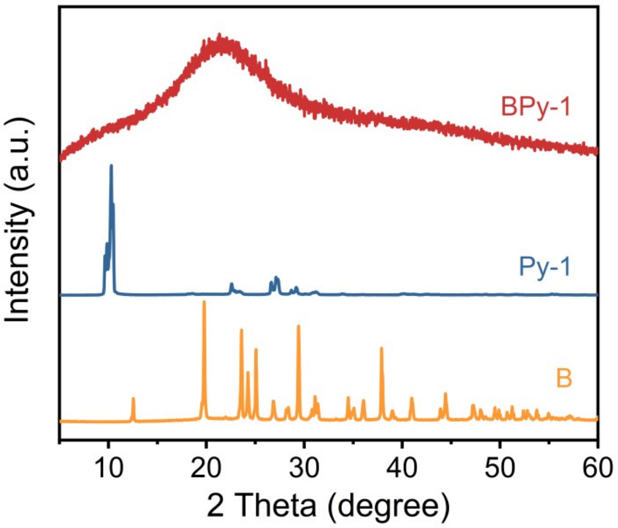

Fig. S15. The XRD patterns of BPy-1 and corresponding precursors (Py-1 and B).

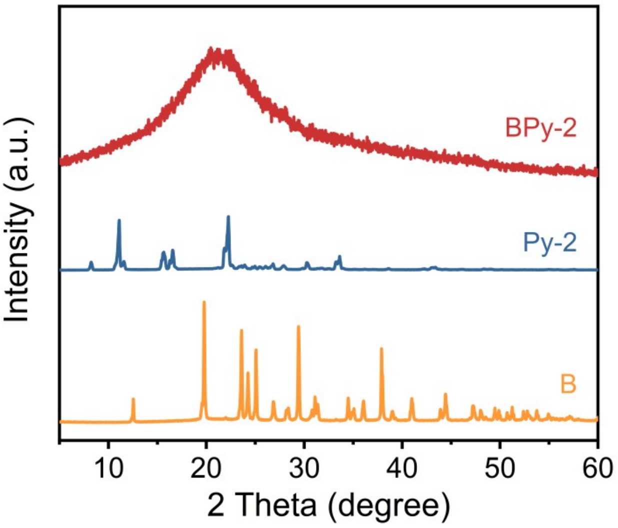

Fig. S16. The XRD patterns of BPy-2 and corresponding precursors (Py-2 and B).

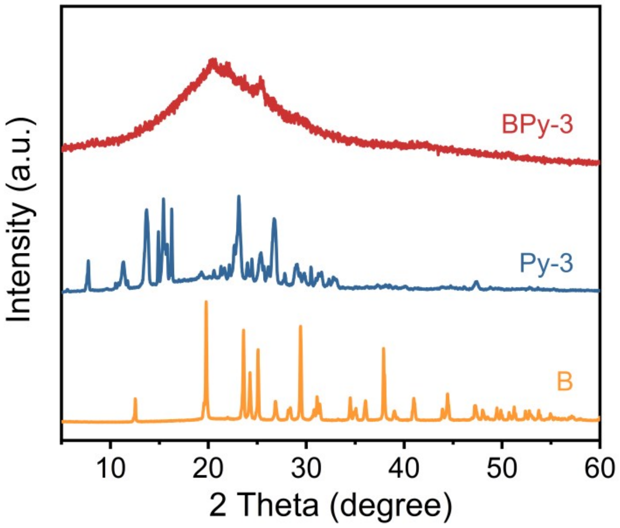

Fig. S17. The XRD patterns of BPy-3 and corresponding precursors (Py-3 and B).

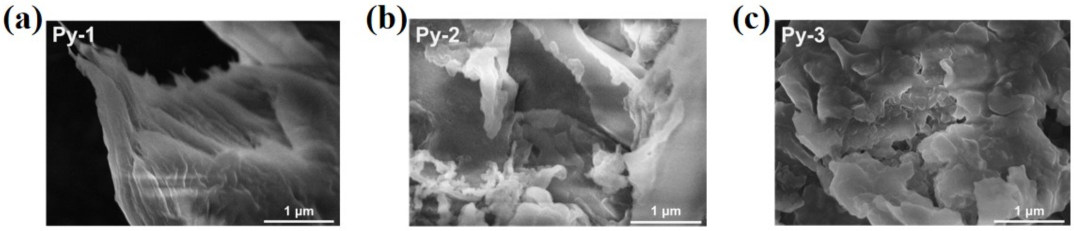

Fig. S18. SEM images of (a) Py-1; (b) Py-2 and (c) Py-3.

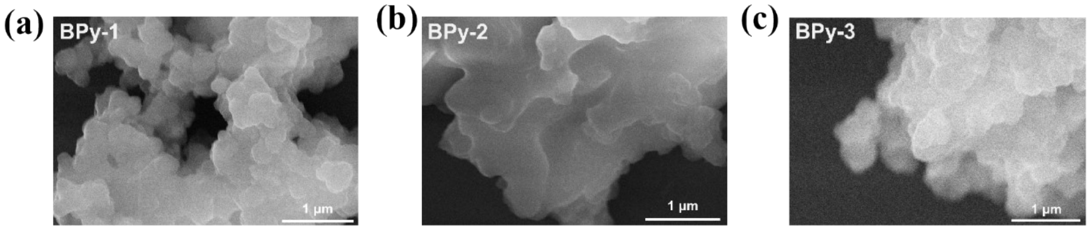

Fig. S19. SEM images of (a) BPy-1; (b) BPy-2 and (c) BPy-3.

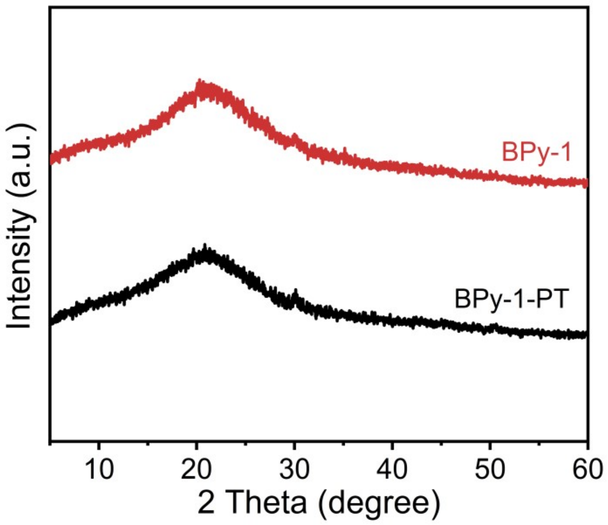

Fig. S20. The XRD patterns of BPy-1 and BPy-1-PT.

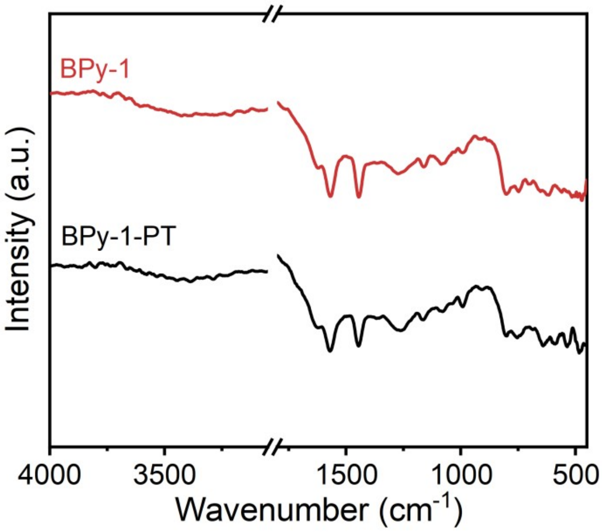

Fig. S21. The FTIR patterns of BPy-1 and BPy-1-PT.

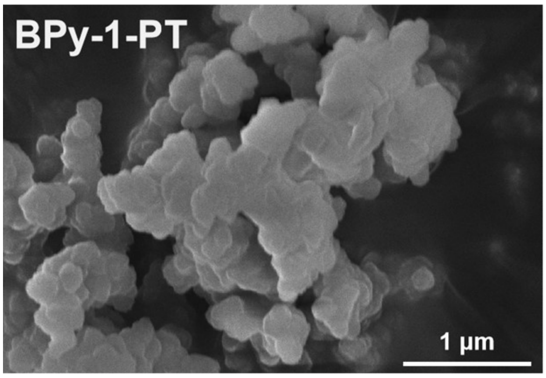

Fig. S22. SEM images of BPy-1-PT.

4. ^{1}H NMR and ^{13}C NMR spectra of Py-X

Fig. S23 to Fig. S28 show the liquid ^{1}H NMR and ^{13}C NMR spectra of Py-X, which ensure the accuracy of the proposed structure of BPy-X.

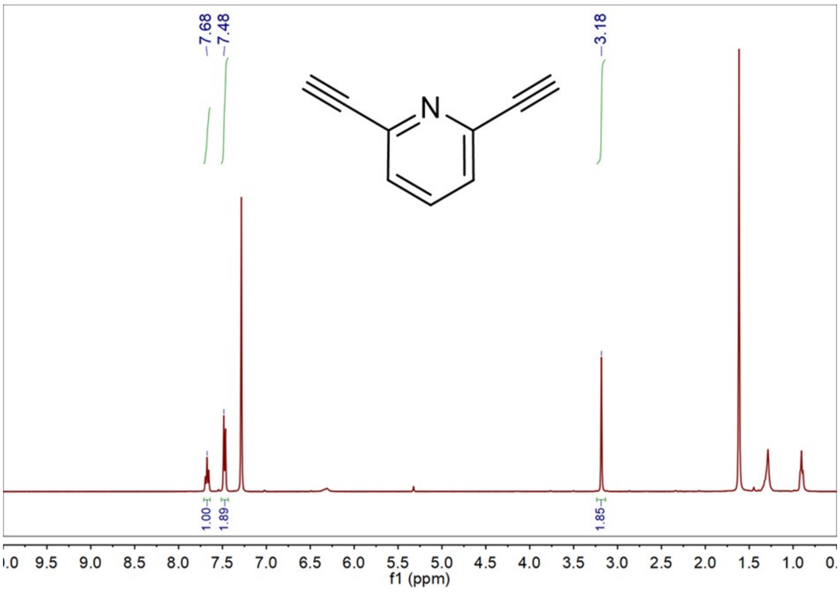

Fig. S23. ^{1}H NMR test results of Py-1 (400 MHz, $CDCl_3$, 298 K): δ (ppm) 7.68 (t, 1H), 7.48 (d, 2H), 3.18 (s, 2H).

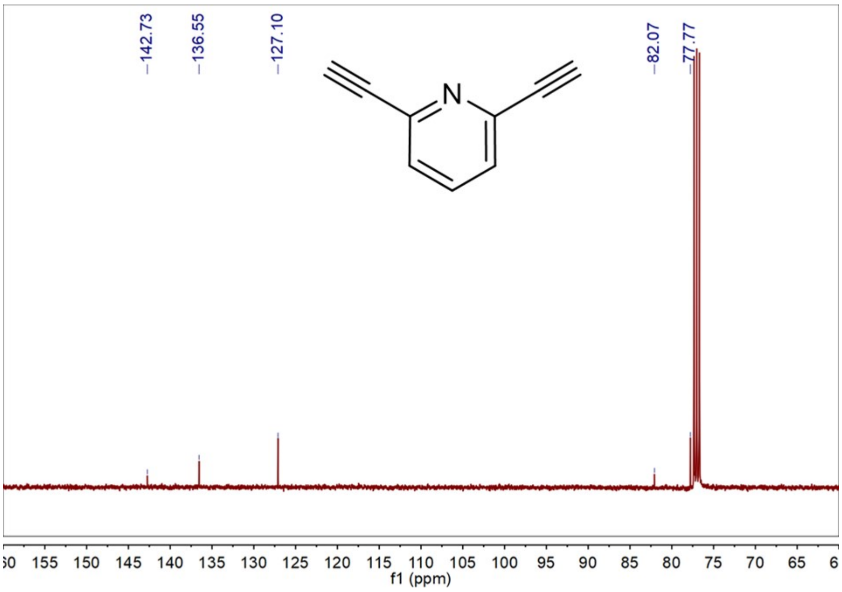

Fig. S24. ^{13}C NMR test results of Py-1 (400 MHz, $CDCl_3$, 298K): δ (ppm) 142.7, 136.6, 127.1, 82.1, 77.8.

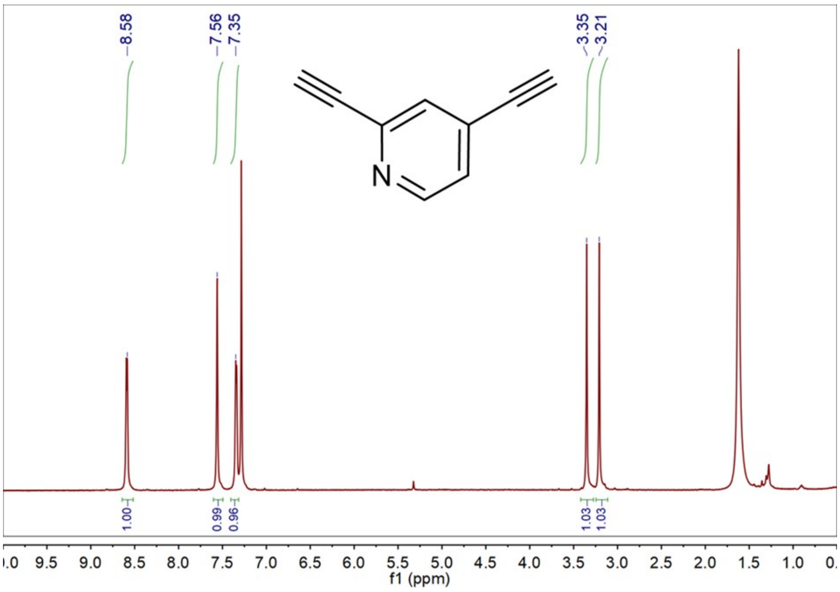

Fig. S25. ^{1}H NMR test results of Py-2 (400 MHz, $CDCl_3$, 298 K): δ (ppm) 8.58-8.56 (dd, 1H), 7.56-7.55 (t, 1H), 7.35-7.33 (dd, 1H), 3.35 (s, 1H), 3.21(s, 1H).

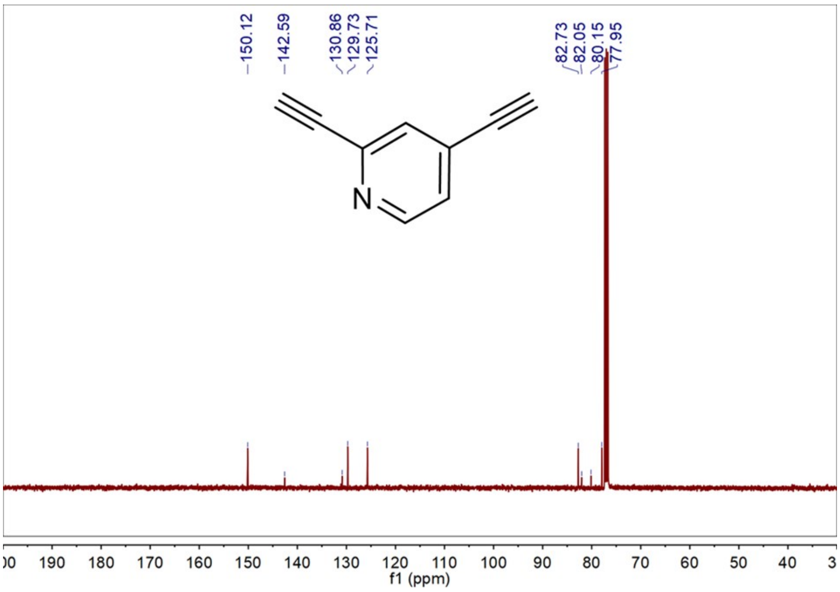

Fig. S26. ^{13}C NMR test results of Py-2 (400 MHz, $CDCl_3$, 298K): δ (ppm) 150.1, 142.6, 130.9, 129.7, 125.7, 82.7, 82.1, 80.2, 78.0.

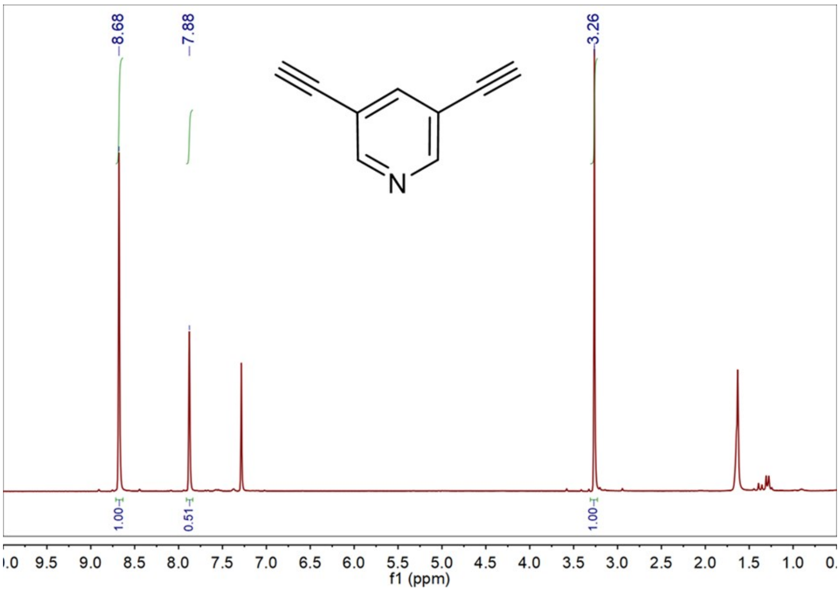

Fig. S27. ^{1}H NMR test results of Py-3 (400 MHz, $CDCl_3$, 298 K): δ (ppm) 8.68 (d, 2H), 7.88 (t, 1H), 3.26 (s, 2H).

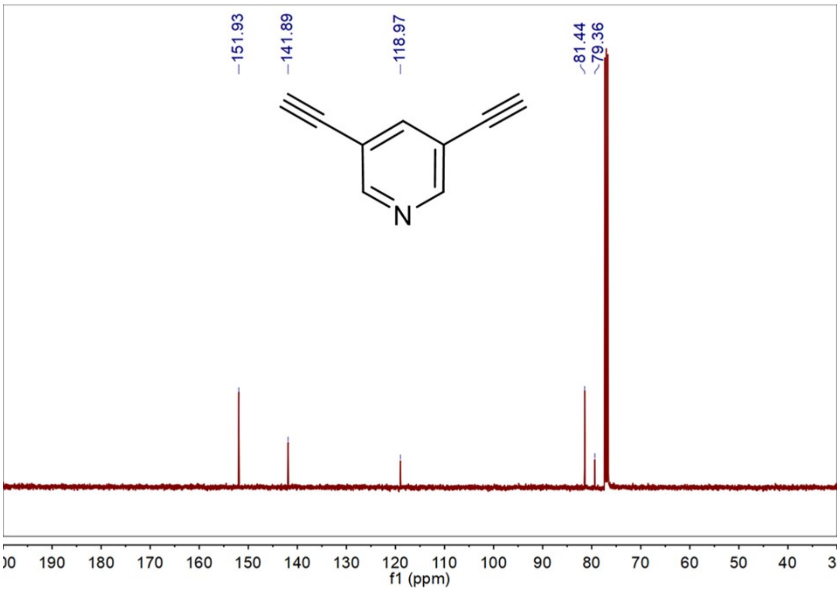

Fig. S28. ^{13}C NMR test results of Py-3 (400 MHz, $CDCl_3$, 298K): δ (ppm) 151.9 141.9, 119.0, 81.4, 79.4.

5. References

1. G. Frisch, H. Schlegel, G. Scuseria, M. Robb, J. Cheeseman, G. Scalmani, V. Barone, G. Petersson, H. Nakatsuji, X. Li, M. Caricato, A. Marenich, J. Bloino, B. Janesko, R. Gomperts, B. Mennucci, H. Hratchian, J. Ortiz, A. Izmaylov, J. Sonnenberg, D. Young, F. Ding, F. Lipparini, F. Egidi, J. Goings, B. Peng, A. Petrone, T. Henderson, D. Ranasinghe, V. Zakrzewski, J. Gao, N. Rega, G. Zheng, W. Liang, M. Hada, M. Ehara, K. Toyota, R. Fukuda, J. Hasegawa, M. Ishida, T. Nakajima, Y. Honda, O. Kitao, H. Nakai, T. Vreven, K. Throssell, J. A. Montgomery, J. Peralta, F. Ogliaro, M. Bearpark, J. Heyd, E. Brothers, K. Kudin, V. Staroverov, T. Keith, R. Kobayashi, J. Normand, K. Raghavachari, A. Rendell, J. Burant, S. Iyengar, J. Tomasi, M. Cossi, J. Millam, M. Klene, C. Adamo, R. Cammi, J. Ochterski, R. Martin, K. Morokuma, O. Farkas, J. Foresman, and D. Fox, *Gaussian 16, Revision C.01; Gaussian, Inc.: Wallingford CT*, 2016.

2. K. Raghavachari, *Theor. Chem. Acc.*, 2000, **103**, 361-363.